Available online at https://doi.org/10.36303/SATNT.2021cosaami.25
*Conference of the South African Advanced Materials Initiative*

# Induction melting of an Al-50Cu alloy for improved homogeneity required for powder spheroidisation

**R van der Merwe[1,a,*], H Bissett[1,b], IJ van der Walt[1,c] and LA Cornish[2,d]**

[1] *The South African Nuclear Energy Corporation SOC Ltd. (Necsa), Elias Motsoaledi Street Extension (Church Street West) R104 Pelindaba, Madibeng Municipality, North West Province, 0240, South Africa*
[2] *School of Chemical and Metallurgical Engineering, and DSI-NRF Centre of Excellence in Strong Materials hosted by the University of the Witwatersrand, Johannesburg, South Africa*
*Email: [a] Ryno.vandermerwe@necsa.co.za[*], [b] Hertzog.bissett@necsa.co.za, [c] Jaco.vanderwalt@necsa.co.za, [d] Lesley.Cornish@wits.ac.za*

## Abstract

Copper alloys are typically produced by conventional casting processes, including spark plasma sintering (SPS), which often produce inhomogeneous mixtures of Cu or Al precipitates and unwanted intermetallic phases in solid products. Induction melting should provide good mixing, controlled heating and melt stirring, potentially improving homogeneity. Homogeneous melts should produce homogeneous powders, giving better properties in additive manufacturing (AM). To ascertain homogeneity, a density test was developed. After comminution, homogeneous powders can be used to produce high quality components. To manufacture dense AM components, spheroidised powders are needed because they increase particle packing and powder flow.

An Al-50Cu (at.%) button was produced by high-frequency (HF) induction melting, to give better mixing and hence phase distributions. To identify the phases and their distributions, the as-cast sample was studied using scanning electron microscopy (SEM), energy dispersive X-ray spectroscopy (EDX) and X-ray diffraction (XRD), as well as absolute density using helium pycnometry. Results indicated inhomogeneity in the samples, due to Al loss, complex solidification and the densest phase settling at the bottom of the button.

**Keywords:** Cu-Al button, Induction melting, homogeneity, spheroidisation

## 1. Introduction

Additive Manufacturing builds components layerbylayer from a three-dimensional (3D) design to achieve complex structures. The most widely utilized materials in AM industries are aluminium alloys, although aluminium-copper alloys also account for a large proportion.[1] Due to their high performance and light weight, Al-Cu components are used in medical, aerospace and automotive sectors.[1] Aluminium has a low density, while copper has a high heat dissipation capacity, making the alloys suitable for various industrial applications.[2] Alloy hardness usually increases with decreasing grain size at ambient temperature.[3] Also, increased Cu content usually increases the hardness values up to a peak, while increased θ $CuAl_2$ proportion increases brittleness.[4] Kim et al.[2] found maximum hardness at ~50 vol. % Cu for spark plasma sintered samples with only θ and γ' phases.

A variety of Cu-Al alloys can be obtained by: melting elemental powders, stir casting,[6] high fusion frequency melting under vacuum of prior cold compacted mixed powders,[4] or spark plasma sintering of mixed elemental powders.[2] The high quality spherical powders required for AM need to be produced from high quality stock, which in this case is a Cu-Al button. A major factor in ensuring that a high quality button is produced is its homogeneity. A cast button is usually considered homogenous if it is mainly single-phase, e.g. >90% η′, or even if the multiple phases in the button are

**Table 1:** Crystal structures of selected intermediate phases of the Cu-Al system[7-11]

| Phase | Chemical formulae | Pearson symbol | Structure type | Temperature range (°C) | Cu composition range (at.%) | Other supporting references |
|---|---|---|---|---|---|---|
| (Al) | Al | *cF*4 | Cu | ≤660.5 | 0-2.48 | [8] |
| θ | $CuAl_2$ | *tI*12 | $Al_2Cu$ | ≤590.5 | 32-36 | [8], [9] |
| η | CuAl | *oP*16/ *oC*16 | n.a. | 573.9-624.5 | 49.8-52.4 | [8] |
| η′ | CuAl | *mC*20 | AlCu | ≤574.5 | 49.8-52.3 | [8], [9] |
| ζ | $Cu_5Al_3$ | *Imm*2 | $Al_3Cu_{4-\delta}$ | 507-597<br>Min. 400-570 | 54.5-56.5<br>55.2-56.7 | [8], [10], [11] |
| ζ′ | $Cu_4Al_3$ | *Fmm*2 | $Al_3Cu_4$ | 298-561<br>530-590 | 56.3-57.4<br>55.2-56.3 | [8], [10], [11] |
| ε′ | $Cu_3Al_2$ | *hP*4 | NiAs | 846-568.5 | 55.0-61.1 | [8] |
| (Cu) | Cu | *cF*4 | Cu | ≤1083 | 80.3-100 | [8] |

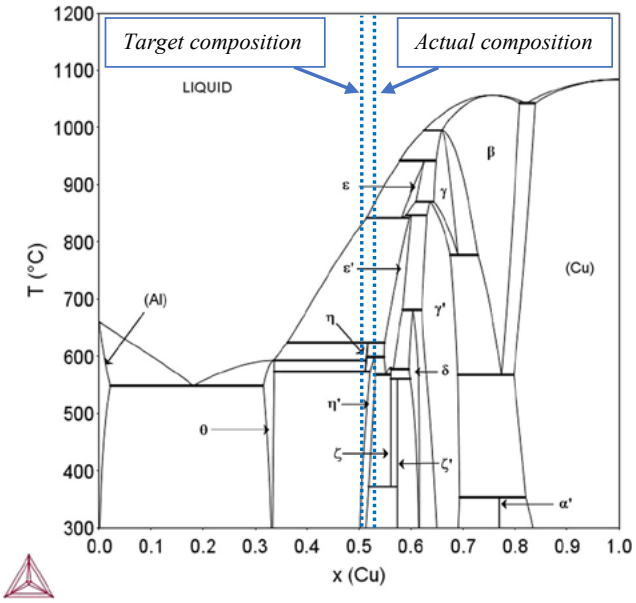


**Figure 1:** Cu-Al phase diagram (Kroupa et al.)[7]

evenly distributed throughout. Powders used for AM are spherical to ensure good flow and good packing, so most powders are either gas (more common) or plasma atomised.[5] Powders treated by plasma spheroidisation are superior in purity and roundness and should not be porous.

An Al-50 at.% Cu button was produced by HF induction melting in a graphite crucible, followed by rapid cooling. As well as studying the phases in the button and powder produced from it by SEM and XRD, a density test was attempted to ascertain whether the targeted η' single phase (Figure 1) had been obtained

## Cu-Al intermetallic compounds

The most recent, thermodynamically reassessed Al-Cu phase diagram by Kroupa et al.[7] is given in Figure 1 and the crystal structures most relevant to this study are given in Table 1.

Hardness of the Al-50Cu button was important, since harder alloys are typically more brittle, usually giving finer particles on comminution, whereas softer alloys are more ductile, usually producing larger particles. Thus, a harder Cu-Al alloy was targeted to potentially produce finer powders, which are optimum feeds for the spheroidisation process, and Kim et al.[2] showed that Al-50Cu should have the highest hardness (~150 HV) to produce satisfactory feed powder for spheroidisation after comminution.

## HF induction melting and plasma spheroidisation

HF induction heating magnetically induces an electrical current into a conductor, and heats the conductor due to its resistivity, with an inherent stirring effect which is similar to the rotation of a motor within its magnetic field.[12]

Thermal plasmas have extremely high temperatures (3000-0 000 K) and rapid heating and cooling rates (~$10^6$ K/s) so are suitable for treating powders at high temperatures, followed by rapid quenching. Plasma spheroidisation involves rapid reshaping and densification of irregularly shaped particles to obtain spheroidised powders.[13]

# 2. Experimental method

## Materials

High purity aluminium (99%) granules from Merck CC, and copper sectioned from old plasma anodes (99.9±0.6%) were cleaned with analytical grade ethanol before use. Argon (99.999 % purity, from Air products, South Africa) provided the inert glove box atmosphere for induction melting and chill casting.

## Induction melting

The Cu and Al metal pieces for a 50 g Al-50Cu button were weighed before induction melting using the conditions provided in Table 2.

**Table 2:** Conditions for induction melting tests

| Condition | Values |
|---|---|
| Melting temperature | 1192ºC-1200ºC |
| Reactor | 50 ml graphite crucible |
| Induction power input | 1541 Watt |
| **Variables** | **Values** |
| Density of pure η′ | 5.36[14] |
| Pressure | <100 kPa (slightly + pressure in glovebox) |

Aluminium was melted first and the temperature increased to 700ºC, then Cu was added and the temperature increased to 1200ºC, where all Cu pieces were observed to melt. As per the standard procedure, the melt was stirred by induction eddy currents for ~5 min before being chill-cast in a water-cooled copper crucible directly beneath.

## Spheroidisation

The chill-cast button was crushed and ground to a powder of <106 µm with a porcelain mortar and pestle, then separated into two size fractions, ≤45 µm and 45 to 90 µm, with a 45 µm and 90 µm sieve stack and a Pascal Sieve Shaker. Particle size analyses of the feed and plasma treated (PT) powders were conducted by laser light scattering with a Saturn DigiSizer II Analyzer.

A 15 kW Tekna PL-35M induction plasma spheroidisation apparatus was used with pure argon (99.999 %) as the central gas at 10 slpm (standard litres per minute); with the sheath gas at 40 slpm and the carrier gas at 2 slpm. The plasma conditions are given in Table 3. Since plasma treatment in the inert atmosphere removes the particles' natural oxide layers, which could make the fine particles pyrophoric and prone to rapid oxidation (even explosion) on exposure to air, the densified/spheroidised powders were slowly passivated by adding air to the surrounding gas mixture before being safely removed from the reactor.

**Table 3:** Thermal plasma conditions treatments of the two powder size fractions, for ~0.4 kg/h powder feed rate and 85 kPa (abs) reactor pressure

| Fraction (µm) | Plasma plate power (kW) | Energy consumption (kW.h / kg) |
|---|---|---|
| ≤45 | 9 | 25.00 |
| 45-90 | 10 | 30.30 |

## Induction melted button

The button was cut in half, using a Struers Accutom-100 cutter with an alumina blade. A 3 mm thick slice was cut from one half (Figure 2), and the other half was halved, with one piece used for SEM-EDX and XRD analyses and the other for spheroidisation. X-ray diffraction was done on the button and powders, using a Bruker D8 Advance diffractometer with Cu $K_\alpha$ ($\lambda$=0.15418 nm radiation) source and a LynxEye position sensitive detector, with results compared against the 2007 PDF-2database to identify the phases. Six points were analysed over the cross-section.

A vertical slice from the centre of the button was mounted in non-conductive Struers Epofix resin and prepared metallographically, polishing the surface to a 1 µm surface finish on a Struers Tegraforce-5, and then carbon-coated (since the system had been calibrated with pure Cu coated with a 50 nm layer of carbon, and the mounting medium was not conductive) for analysis. Samples were examined using an FEI Quanta 200 3D SEM with an EDAX Octane Elect energy dispersive X-ray spectroscope (EDS). Each analysis was on a 1 x 1.2 mm area at the lowest magnification (155x). The positions of the areas analysed by SEM were similar to the pattern of the XRD point analyses (inset in Figure 2)-

Two thirds of the 10 ml sample chamber of the pycnometer was filled by different samples, which had been weighed before: 13.4 g for the Al-50Cu button piece, 29.5 g for pure Cu and 10.7 g for pure Al. Density analyses were performed in triplicate at an equilibration rate of 0.345 kPa/min. The crystal density for a η· phase sample was calculated from its unit cell and lattice parameters.[14] The statistical difference between the measured button density and calculated η′ density was determined by a Student's t-test.[15]

## Spheroidised powders

Secondary electron (SE) images were image processed using the Carl Zeiss Zen 2 Core software package to determine particle morphologies for different plasma conditions, by deriving average circularities (shape factor) of whole particles. A circularity value of 1 is true circle.[16] Although circularity is two dimensional, and sphericity is three dimensional, particles having a circularity value of ≥0.85 were defined as spherical.[17] The "spheroidisation ratio" was the proportion of spherical particles in the total number of particles counted. The phases of the feed and plasma treated powders were determined by X-ray diffraction similar to those in the button.

# 3. Results

## Sample homogeneity

Figure 2 shows overlaid XRD patterns from the six spots on the cross-section of Al-50Cu. Table 4 shows the induction melted button and plasma-treated powders had the same phases: θ, ε′ and η′, but with different phase proportions. It was not possible to distinguish between η′ and η using XRD (because the distinguishing peaks are at lower intensities). Preferred orientation was indicated by the peak intensities not matching the reference patterns [2007 PDF-2database], so phase proportions could not be calculated using Rietveld (or similar) analysis.

**Table 4:** XRD results of the induction melted button and plasma-treated powders

| Phase | Approximate proportions from middle micrograph (%) | Phase reference [2007 PDF-2database) |
|---|---|---|
| ε′ | 75 | 01-074-7053 |
| η′ | 20 | 00-026-0016 |
| θ | 5 | 00-026-0015 |

The major phase throughout the button cross-section was ε′, with less θ, and η′ (Figure 3a). The button composition, derived from areal analyses at the minimum magnification (155x), were similar across the cross-section. Since no pores were observed in the SE image (Figure 3b), the sample was suitable for density measurements using a pycnometer. In a product with closed porosity (e.g. from SPS), helium from the pycnometer could not reach and fill those pores effectively, leading to a significantly lower measured density

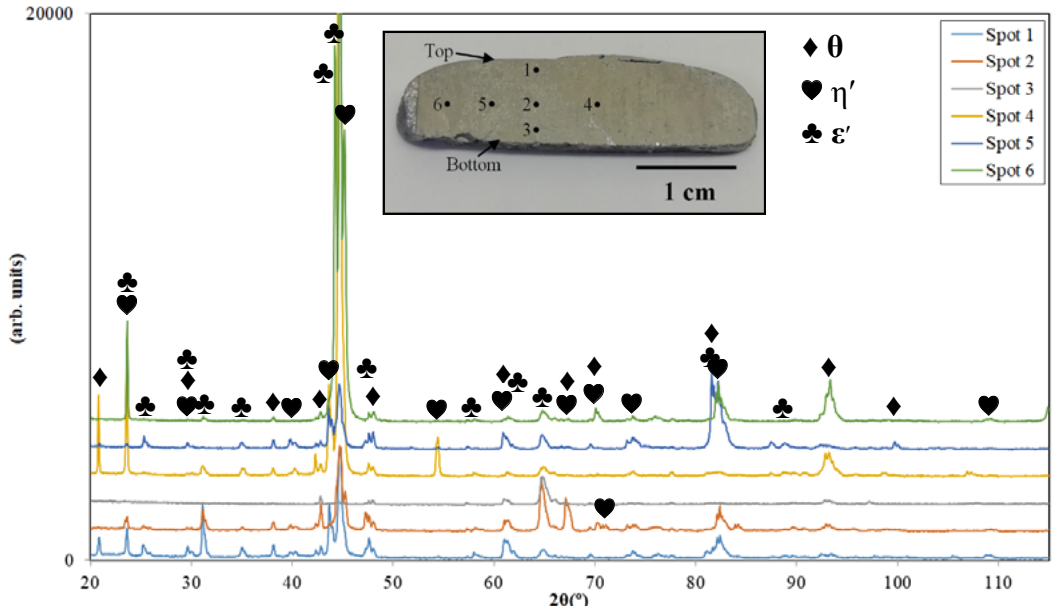


**Figure 2:** X-ray diffraction patterns of six spots on the cross-section of button Al-50Cu

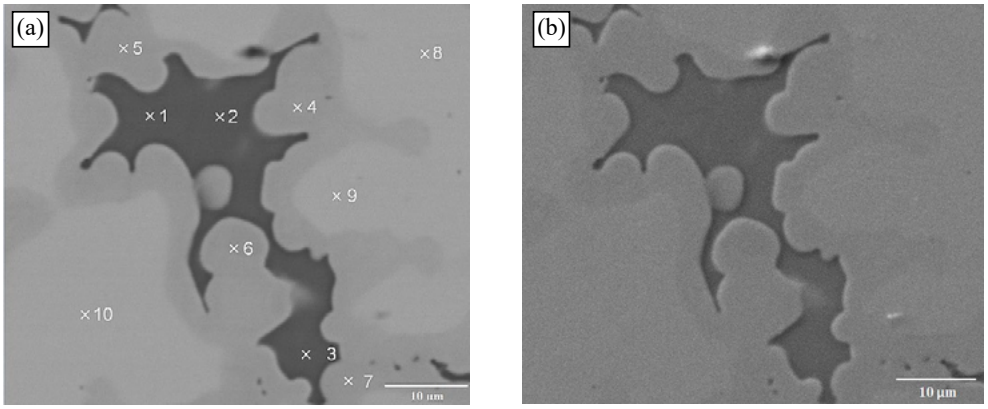


EDX spot analyses at the centre of the Al-50Cu button.

| Spots | Cu (at.%) | Possible phase |
|---|---|---|
| 1-3 | 33.3±0.3 | θ |
| 4-7 | 51.8±0.4 | η / η′ |
| 8-10 | 55.5±0.1 | ε′ |
| Areal analysis (at 155x magnification) | 52.3±0.3 | ε′ + η / η′ + θ |

**Figure 3:** Electron micrographs of the Al-50Cu button centre: (a) SEM-BSE image with EDX spot positions, showing ε′ (light contrast), η′ (medium contrast) and θ (dark contrast) and (b) SEM-SE image indicating no porosity

than that of the pure phase. Crystallographic densities for the Cu-Al compounds are shown in Table 5.

## Spheroidised powders

Figure 4 shows the XRD patterns of the spheroidised Al-50Cu feed powders for the two size fractions in Table 6.

Figure 5 shows the feed and plasma treated powders. Table 6 shows the spheroidisation ratios, obtained from image processing of Figure 5, for powders treated at 9 kW and 10 kW. Table 6 also lists the measured parameters before and after plasma treatment. Average circularity of the ≤45 µm powder increased after plasma treatment from 0.794 to 0.859.

# 4. Discussion

## Sample homogeneity

The major phase in the Al-50Cu button was not η′ (Table 2), since Al was lost during melting due to its higher vapour pressure than copper (0.82 kPa for Al and 0.51 for Cu at 1200ºC).[18] Thus, it would have been better to have melted at a lower temperature. Although the targeted composition was not achieved, the same phases were produced across the button after induction melting,

**Table 5:** Density determination of Al-50Cu alloy button and plasma treated powders (PTP)

| Sample (Name) | Phase | pure phase ρ (g/cm³) | Measured ρ (g/cm³) | Student's t-test*[15] ($t_{experimental}$) | Statistically significantly different (> $t_{critical}$) |
|---|---|---|---|---|---|
| Pure Al | Al | 2.70 | 2.7078±0.005 | 2.21 | No |
| Al-50Cu | η′ | 5.36 | 5.6160±0.003 | 120.68 | Yes |
| ≤45 µm feed powder | η′ | 5.36 | 5.7042±0.056 | 8.66 | Yes |
| ≤45 µm PTP | η′ | 5.36 | 5.8192±0.073 | 8.93 | Yes |
| 45-90 µm feed powder | η′ | 5.36 | 5.6027±0.008 | 42.90 | Yes |
| 45-90 µm PTP | η′ | 5.36 | 5.4367±0.007 | 15.50 | Yes |
| Pure Cu | Cu | 8.96 | 8,9660±0.002 | 3.54 | No |

*All $t_{experimental}$ values were calculated using 2 degrees of freedom and $t_{critical}$ was for the 95% confidence interval (4.303).

**Table 6:** Average circularity and spheroidisation (obtained from image processing) and the median particle size (obtained from laser light scattering) of the feed and PT powders

| Fraction (µm) | Energy consumption (kW.h / kg) | Number of particles measured | Spheroidisation ratio (%) | Average Circularity | Median particle size (µm) |
|---|---|---|---|---|---|
| Feed: ≤45 | 0 | 0 | 0 | 0.773±0.070 | 33.41±0.49 |
| PT: ≤45 | 25.00 | 222 | 35 | 0.809±0.086 | 20.64±2.73 |
| Feed: 45-90 | 0 | 0 | 0 | 0.758±0.071 | 74.98±0.31 |
| PT: 45-90 | 30.30 | 87 | 48 | 0.842±0.106 | 46.58±0.32 |

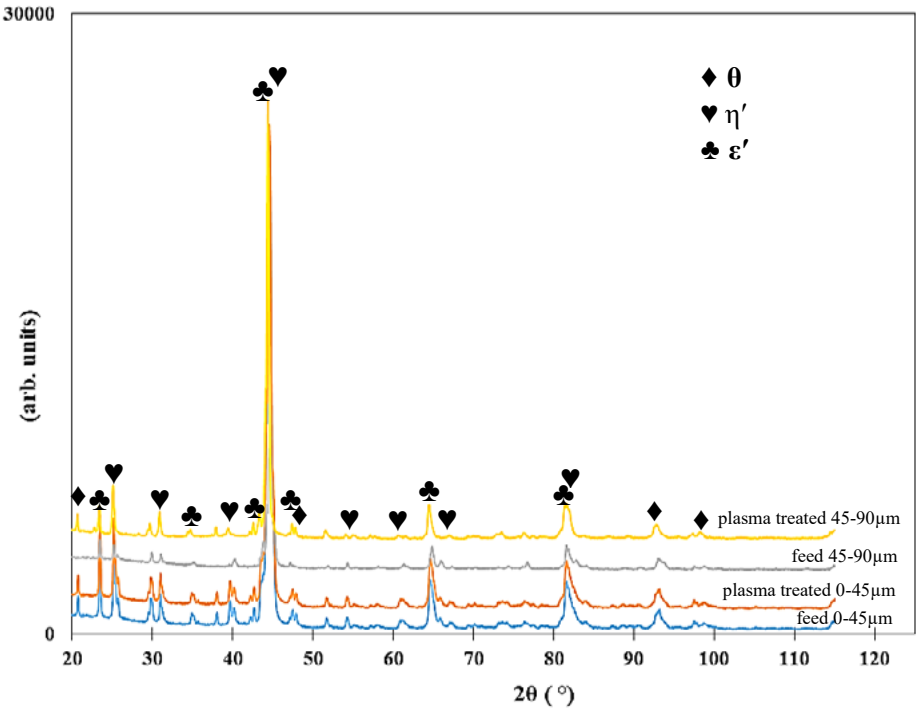


**Figure 4:** X-ray diffraction patterns of Al-50Cu powders

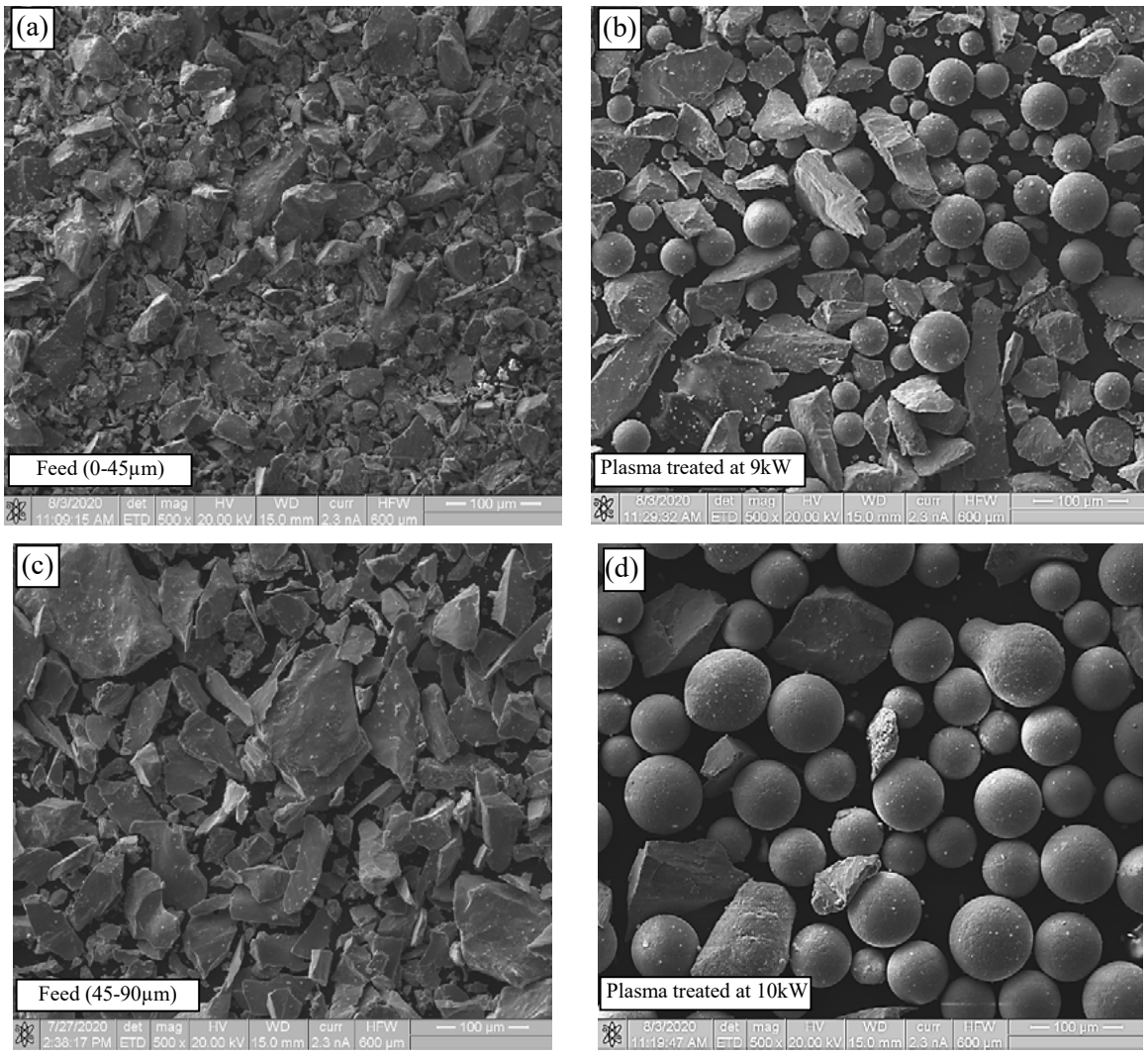


**Figure 5:** SEM-SE images of the Al-50Cu powder: (a) ≤45 µm feed powder, (b) ≤45 µm powder treated at 9 kW, (c) 45-90 µm feed powder and (d) 45-90 µm powder treated at 10 kW

albeit in different proportions. It is unlikely from the phase diagram[7] that only η′ would be produced on solidification, because there are higher temperature phases that solidify first, with no direct solidification to η′ (although there is direct solidification to η). Thus, heat treatment would be necessary around 500°C to attempt to form η′.

Rapid cooling from chill casting gave non-equilibrium conditions, which retained some of the higher temperature phases. From the microstructure, EDX (Figure 3) and XRD (Figure 2), the phase formation order was ε′, η′ and θ. There might have been direct solidification to ε, but the high temperature peritectic reaction at 846°C is likely to have gone to completion, then ε′ would have solidified directly (Figure 1, Table 1)[7], then undergo a peritectic reaction ($L + \varepsilon' \rightarrow \eta$) to form some η at 624.5°C,[7] which was subsequently involved in another peritectic reaction ($L + \eta \rightarrow \theta$)[7] at 590.5°C[7] to form θ. This last reaction occurred because of the rapid cooling, so that the liquid ran down the liquidus until it reached that reaction. This can occur in fast cooling with successive peritectic reactions,[19] and would preclude phases with higher Cu contents than those already solidified.

The two different powder sizes had similar compositions for the feed and plasma treated samples. However, at the button centre (Figure 2: Spot 4) the less dense η′ was the major phase. Since the density of Cu is nearly 3.3 times that of Al, the denser ε′ (higher Cu content) was expected to sink to the bottom of the melt (Figure 2: Spot 3), but did not since the phase distribution was improved by stirring and levitation induced by HF induction overcoming the density differences. The different relative intensities (Figure 2) indicated the phase proportions differed across the sample, although the preferred orientation made comparison difficult.

Only the pure Al and Cu samples had statistically significantly different (Student's t test) densities, because the samples comprised one element (Table 5). The alloy button and powders had statistically significantly different densities from the targeted η′ (Table 5), because they were multi-phase (Figures 2 and 4). Since the phase proportions varied across the sample, the EDX analysis of the button (Figure 3) was not used to derive the button/powder densities. Thus, the Student's t-test (Table 5) was a pass/fail criterion depending on whether the button/powders densities agreed with the targeted η′ phase.

The measured density of the feed powder was significantly lower than the calculated value (Table 6) due to the elongated particles formed by comminution (Figures 5a and c). Plasma treatment spheroidised and decreased the median particle volume, so the powder density increased.

## Spheroidised powders

The ≤45 µm and 45-90 µm feed powder particles were irregularly shaped (Figures 5a and c), and were successfully spheroidised (Table 6, Figure 5b and d). However, the ≤45 µm powder treated at 9 kW had fewer fine particles (<1 µm) (Figure 5), as large particles melt and fine particles evaporate, from the minimum energy transfer to melt a particle, Equation 1:[13]

$$P = \dot{m} [c_p (T_m - T_0) + H_m] \quad (1)$$

where P = minimum energy per unit time required (W), $\dot{m}$ = powder feed rate (g/s), $c_p$ = specific heat capacity (J/K.g), $T_m$ = melting point, $T_0$ = room temperature, and $H_m$ = latent heat of fusion (J/g) of the powder treated.[20] For a single particle, the mass (m) can be substituted by $1/6\pi d^3$ where d = particle diameter. Thus, the minimum energy to melt a particle depends on particle size, with more energy required to melt larger particles. For fine particles, evaporation might occur if more energy was available during spheroidisation. Thus, for effective spheroidisation without evaporation, the particle size distribution of the feed powder should be as narrow as possible, since more evaporation occurs from finer particles with higher surface:volume ratios.

More energy was used for the spheroidisation of the larger size fraction (Table 6), giving a higher spheroidisation ratio. Although the average circularity increased from 0.76-0.77 to >0.8 (Table 6), many particles were considered irregular (circularity of ≥0.85 was considered spherical). Although the average circularity increased, the decrease in the median particle size indicated that material evaporated and condensed as fine particles, decreasing the median particle size after plasma treatment (Table 6).

## 5. Conclusions

- Spot (SEM-EDX and XRD) and bulk (density) analyses of the Cu-Al button and spheroidised powders proved that the density measurements could be used for ascertaining the homogeneity of small induction melted buttons.
- The Al-50Cu button produced was not homogeneous, with varying proportions of ε′, η′ and θ phases, as shown by SEM-EDX and XRD.
- Densities of the button and powders deviated from the targeted η′ phase due to Al evaporation during induction melting and plasma treatment, giving an excess of Cu and solidification of the higher density ε′ phase as the major phase. A minimum temperature of 950ºC with longer holding there would have allowed the source copper to thoroughly melt, reduce Al evaporation and produce a more homogeneous product. Heat treatment around 500°C would have improved the η′ proportion.
- Ground powders were irregularly-shaped, although plasma processing improved spheroidisation. The 45-90 µm powder had the highest spheroidisation ratio (48 %), from higher plasma energy inputs. Overall, the median particle size decreased after spheroidisation due to fine particle formation.

## Acknowledgements

Grateful acknowledgement is due to: Department of Science and Innovation (DSI), through the Advanced Material Initiative (AMI) and the South African Nuclear Energy Corporation (Necsa) for financial support; Nuclear Materials (NM) and the Plasma Technology sections in the Applied Chemistry (AC) department, Research and Development Division at Necsa for the use of their facilities; and Necsa personnel: Dr S.J. Lotter (SEM), Dr T.P. Ntsoane (XRD), and Mr M.M. Makhofane and Mr P.C. Smith (plasma experiments).

## References

1. N. T. Aboulkhair, M. Simonelli, L. Parry, I. Ashcroft, C. Tuck, and R. Hague, '3D printing of Aluminium alloys: additive manufacturing

of Aluminium alloys using selective laser melting', *Prog. Mater. Sci.*, vol. 106, p. 100578, Dec. 2019, doi: 10.1016/j.pmatsci.2019.100578.

2. K. Kim, D. Kim, K. Park, M. Cho, S. Cho, and H. Kwon, 'Effect of intermetallic compounds on the thermal and mechanical properties of Al–Cu composite materials fabricated by spark plasma sintering', *Materials*, vol. 12, no. 9, p. 1546, May 2019, doi: 10.3390/ma12091546.
3. R. W. Armstrong, '60 Years of Hall-Petch: Past to present nano-scale connections', *Mater. Trans.*, vol. 55, no. 1, pp. 2–12, 2014, doi: 10.2320/matertrans.MA201302.
4. N. Boukhris, S. Lallouche, M. Y. Debili, and M. Draissia, 'Microhardness variation and related microstructure in Al–Cu alloys prepared by HF induction melting and RF sputtering', *Eur. Phys. J. Appl. Phys.*, vol. 45, no. 3, p. 30501, Mar. 2009, doi: 10.1051/epjap/2009016.
5. A. Cooke and J. Slotwinski, 'Properties of metal powders for additive manufacturing: A review of the state of the art of metal powder property testing', National Institute of Standards and Technology, NIST IR 7873, Aug. 2012. doi: 10.6028/NIST.IR.7873.
6. T. Balarami Reddy, P. Karthik, and M. Gopi Krishna, 'Mechanical behaviour of Al–Cu binary alloy system/Cu particulates reinforced metal-metal composites', *Results Eng.*, vol. 4, p. 100046, Dec. 2019, doi: 10.1016/j.rineng.2019.100046.
7. A. Kroupa, O. Zobač, and K. W. Richter, 'The thermodynamic reassessment of the binary Al–Cu system', *J. Mater. Sci.*, vol. 56, no. 4, pp. 3430–3443, Feb. 2021, doi: 10.1007/s10853-020-05423-7.
8. J. L. Murray, 'The aluminium-copper system', *Int. Met. Rev.*, vol. 30, no. 1, pp. 211–234, Jan. 1985, doi: 10.1179/imtr.1985.30.1.211.
9. Y. Funamizu and K. Watanabe, 'Interdiffusion in the Al-Cu System', *Trans. Jpn. Inst. Met.*, vol. 12, no. 3, pp. 147–152, 1971, doi: 10.2320/matertrans1960.12.147.
10. N. Ponweiser, C. L. Lengauer, and K. W. Richter, 'Re-investigation of phase equilibria in the system Al–Cu and structural analysis of the high-temperature phase $\eta_1$-$Al_{1-\delta}Cu$', *Intermetallics*, vol. 19, no. 11, pp. 1737–1746, Nov. 2011, doi: 10.1016/j.intermet.2011.07.007.
11. O. Zobac, A. Kroupa, A. Zemanova, and K. W. Richter, 'Experimental description of the Al-Cu binary phase diagram', *Metall. Mater. Trans. A*, vol. 50, no. 8, pp. 3805–3815, Aug. 2019, doi: 10.1007/s11661-019-05286-x.
12. M. Mansoor and M. Shahid, 'On the designing, efficiency, and stirring force of an induction coil for the processing of prototype Al based nanocomposites', *J. Metall.*, vol. 2014, pp. 1–6, 2014, doi: 10.1155/2014/637031.
13. M. I. Boulos, P. L. Fauchais, and E. Pfender, *Handbook of Thermal Plasmas*. Cham: Springer International Publishing, 2017. doi: 10.1007/978-3-319-12183-3.
14. M. El-Boragy, R. Szepan, and K. Schubert, 'Kristallstruktur von $Cu_3Al_{2+}$(h) und CuAl (r)', *J. Common Met.*, vol. 29, no. 2, pp. 133–140, Oct. 1972, doi: 10.1016/0022-5088(72)90183-X.
15. Student, 'The probable error of a mean', *Biometrika*, vol. 6, no. 1, p. 1, Mar. 1908, doi: 10.2307/2331554.
16. H. Bissett, M. M. Makhofane, R. van der Merwe, and S. J. Lotter, 'Plasma dissociation of monazite', *IOP Conf. Ser. Mater. Sci. Eng.*, vol. 655, p. 012040, Nov. 2019, doi: 10.1088/1757-899X/655/1/012040.
17. I. Cruz-Matías *et al.*, 'Sphericity and roundness computation for particles using the extreme vertices model', *J. Comput. Sci.*, vol. 30, pp. 28–40, Jan. 2019, doi: 10.1016/j.jocs.2018.11.005.
18. C. B. Alcock, V. P. Itkin, and M. K. Horrigan, 'Vapour pressure equations for the metallic elements: 298–2500K', *Can. Metall. Q.*, vol. 23, no. 3, pp. 309–313, Jul. 1984, doi: 10.1179/cmq.1984.23.3.309.
19. T. D. Boniface and L. A. Cornish, 'Investigation of the aluminium-ruthenium phase diagram above 25 at.% ruthenium', *J. Alloys Compd.*, vol. 234, no. 2, pp. 275–279, Feb. 1996, doi: 10.1016/0925-8388(95)01933-2.
20. X.-L. Jiang and M. Boulos, 'Induction plasma spheroidization of tungsten and molybdenum powders', *Trans. Nonferrous Met. Soc. China*, vol. 16, no. 1, pp. 13–17, Feb. 2006, doi: 10.1016/S1003-6326(06)60003-4.